

# Comparing and Quantifying Indoor Performance of Organic Solar Cells

Dana Lübke, Paula Hartnagel, Johanna Angona, and Thomas Kirchartz\*

With increasing efficiencies of non-fullerene acceptor-based organic solar cells, thin-film technology is becoming a promising candidate for indoor light harvesting applications. However, the lack of standardized comparison methods makes it difficult to quantify progress and to compare indoor performance. Herein, a simple method to calculate the efficiency of solar cells under any possible light source and illuminance with only using simple standard measurements (current–voltage curves and quantum efficiency) is presented. Thereby, equal evaluation conditions are ensured, so that indoor solar cells can be ranked and compared according to their efficiency. Efficiencies are shown to typically vary by  $\pm 20\%$  when using different different light emitting diode spectra with color temperatures ranging from 2700 to 6500 K. Calculations based on a detailed balance model indicate that the optimal bandgap of the absorber material depends on the used light source and ranges between 1.75 and 2 eV. The approach is validated by comparison with literature data and many calculated efficiencies match well with experimental data obtained with a specific light source. However, some reported efficiencies cannot be reproduced with the model, which highlights the need to reassess low light measuring techniques. Furthermore, a script is provided for use by the community.

An important application that benefits from the tuneability of band gaps in molecular semiconductors is the use of organic photovoltaics (OPV) for indoor light harvesting. The market of the internet of things (IoT) is emerging remarkably and demands to drive high amounts of off-grid low power consumption devices.<sup>[8–13]</sup> The possibility to produce solution-based, low-cost, and flexible solar foils makes OPV a good candidate to fulfill this demand. Furthermore, the absorption spectra of the active materials can be tuned chemically to match different light sources.

Although efficiencies for indoor organic photovoltaics (iOPV)<sup>[14–35]</sup> and other emerging indoor photovoltaics (iPV) technologies such as halide perovskites<sup>[36–43]</sup> or dye-sensitized solar cells<sup>[44–50]</sup> have improved substantially, it is hard to quantify progress and determine champion solar cells due to a lack of standardized comparison methods.<sup>[12,51,52]</sup> Different authors use different conditions to evaluate the performance of their devices. The set-ups differ in the illuminance value (ranging typically from 200 to 1000 lux) and the source of light, namely light emitting diodes (LED) or fluorescent lamps (FL) with varying emission spectra and color temperatures. This makes it difficult to compare devices and regularly leads to the publication of tables or figures where data is compared for different input spectra and illuminances.<sup>[43,53,54]</sup> The exact spectrum and intensity are, however, more than just a minor inconvenience for data comparison but can have a major impact on the output power at a given illuminance and the efficiency. This is due to several reasons. First, the presence of shunts<sup>[55–57]</sup> can have a substantial effect on the dependence of open-circuit voltage and fill factor on the light intensity under indoor conditions.<sup>[55,56,58]</sup> Second, the short-circuit current at a given illuminance strongly depends on the overlap of the materials' absorption spectra and the spectral emission power of the light source.<sup>[53,59]</sup> The exact spectrum is even more critical than for outdoor illumination, because indoor light sources have much more narrow spectra with strong emission between wavelengths of 400 and 700 nm<sup>[60,61]</sup> as compared to the air mass 1.5 global (AM1.5G) spectrum.


In the worst-case scenario, an otherwise well-performing solar cell could exhibit low efficiencies if the color temperature of the light source is not suitable to the specific absorber bandgap. Standardizing indoor spectra as done for outdoor efficiency measurements is not practical given the substantial spectral differences between the used light sources. Furthermore,

## 1. Introduction

With the development and application of a broad range of strongly absorbing non-fullerene acceptors in the last 5 years, the power conversion efficiencies of organic solar cells have increased rapidly and are now approaching 20%.<sup>[1–6]</sup> While these efficiencies are still lower than those of crystalline silicon and other inorganic solar cell technologies,<sup>[7]</sup> using organic molecules offers a range of advantages that make those materials attractive for applications other than utility-scale electric supply.

D. Lübke, P. Hartnagel, J. Angona, T. Kirchartz  
IEKS-Photovoltaik  
Forschungszentrum Jülich  
52425 Jülich, Germany  
E-mail: t.kirchartz@fz-juelich.de

T. Kirchartz  
Faculty of Engineering and CENIDE  
University of Duisburg-Essen  
Carl-Benz-Str. 199, 47057 Duisburg, Germany

 The ORCID identification number(s) for the author(s) of this article can be found under <https://doi.org/10.1002/aenm.202101474>.

© 2021 The Authors. Advanced Energy Materials published by Wiley-VCH GmbH. This is an open access article under the terms of the Creative Commons Attribution License, which permits use, distribution and reproduction in any medium, provided the original work is properly cited.

DOI: 10.1002/aenm.202101474

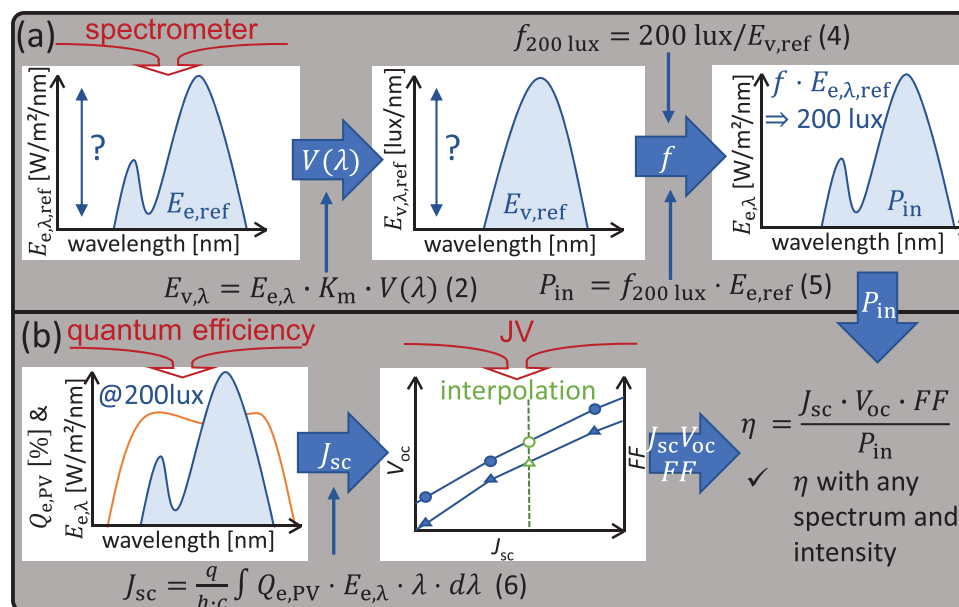


**Figure 1.** Overview to our proposed method, including measurements (red) and calculations (arrows). Details on the normalization of reference spectra to calculate the a) input power are described in Section 2.1 and the determination of the b) output power is discussed in Section 2.2.

the intensity of the emission power determines the input power  $P_{in}$ , that is, the denominator of the efficiency  $\eta = P_{out}/P_{in}$ , where  $P_{out}$  is the output power of the solar cell. Using a lux meter is an easy but highly inaccurate method to test the illuminance<sup>[31,59,62]</sup> and therefore should not be used to evaluate efficiencies in publications. Absolute measurements of the spectral irradiance would be needed to determine precise input powers.

In the literature, several approaches to either analyze the problem or present solutions to the challenge of comparability have been presented in recent years. Chen et al.<sup>[51]</sup> presents a large round robin study on dye-sensitized solar cells reporting relative deviations of indoor reporting relative deviations of indoor efficiencies among different laboratories of up to 152%. Virtuani et al., simulated performance parameters of a copper-poor Cu(In,Ga)Se<sub>2</sub> cell under different indoor illumination levels and spectral distributions.<sup>[52]</sup> A very recent study of Cui et al., aims to provide guidance to a more precise way of measuring indoor efficiencies. They identified different measurement errors, which originate from the use of artificial light sources and measurement methods (temporal stability and spatial inhomogeneities of light sources, edge effects, using lux meters) and proposed practical measuring protocols.<sup>[59,62]</sup> While these studies focus on the conditions and circumstances generated by the use of artificial light sources, a proposed method to quantify and compare (existing) data from different laboratories is still missing.

To address the problem of unavoidable arbitrariness of different light sources one needs to find figures of merits, which are easy to use by the PV community. In this analysis, we present an evaluation method based on the measurement of the external quantum efficiency ( $Q_{e,PV}$ ) combined with relative measurements of the spectral irradiance and current-density-voltage ( $JV$ ) characteristics at different light intensities with one light source. With this combination of relatively simple methods, it is possible to calculate the theoretical efficiency of a solar cell for light sources with different emission spectra and

at different light intensities and thus, enable a fair comparison of the indoor performance of different solar cells. Based on this approach, we present a meta-analysis of the current state of the art iOPV and compare this state of the art with thermodynamic efficiency limits under indoor illumination. Although we focus in this study on the application of our method to OPV, the method can be applied to other PV technologies. Furthermore, we provide a script that allows the community to calculate the efficiencies of their own devices given the above input data. Thereby, our approach does not only provide a solution for researchers, who want to compare their data, but also gives a practical perspective to companies and costumers, who want to choose the optimal absorber blend for a given illumination condition or estimate the needed area for a given power demand of an IoT device.

## 2. Theoretical Background

The determination of photovoltaic power conversion efficiencies depends on the spectrum of the used light source as the efficiency scales inversely with the input power. In Section 2.1, we give the theoretical background to calculate the input power density at a defined illuminance level with a relative irradiance spectrum. In Section 2.2, we demonstrate how to adjust the measured output power of the solar cell to the defined illumination level. Together, Section 2.1 (dealing with the input power of the light source) and Section 2.2 (dealing with the output power of the solar cell) are describing our proposed method, which enables a calculation of the efficiency under any light source spectrum and illuminance intensity with only using standard measuring methods ( $Q_{e,PV}$ ,  $JV$ , and spectrometer). A stepwise instruction on how to use this method and a link to the Matlab code can be found in Section 4 and additionally, **Figure 1** gives an overview on how to use our method. As this method is calculation based, it gives not only the freedom to compare literature

data, but also serves the practical purpose to scan for the best absorber material for a given illumination.

## 2.1. Determination of Input Power Densities at Constant Illuminance

The efficiency  $\eta = P_{\text{out}}/P_{\text{in}}$  is determined by the ratio of the output power  $P_{\text{out}}$  of the solar cell and the input power  $P_{\text{in}}$  from the light source. The integration of the spectral irradiance  $E_{e,\lambda}$  (for indoor applications usually in  $\mu\text{W cm}^{-2} \text{ nm}^{-1}$ ) over the wavelength  $\lambda$  results in the power density or irradiance

$$P_{\text{in}} = E_e = \int E_{e,\lambda} d\lambda \quad (1)$$

of the light source given typically in  $\mu\text{W cm}^{-2}$ . For indoor light applications, photovoltaic performance is usually quantified at a given illuminance, which is a quantity that takes the sensitivity of the human eye into account. Thus, the idea is to compare at an equal brightness perceived by the human observer rather than at a standardized power density as is done for outdoor performance measurements. To determine the illuminance from the power density, we first have to multiply the spectral irradiance  $E_{e,\lambda}$  with the standard sensitivity curve of the human eye  $V(\lambda)$  and the coefficient  $K_m = 683 \text{ lm W}^{-1}$  to arrive at

$$E_{v,\lambda} = E_{e,\lambda} K_m V(\lambda) \quad (2)$$

Here,  $E_{v,\lambda}$  is the spectral illuminance in  $\text{lux nm}^{-1}$ , which then can be integrated as in Equation (1) to obtain the illuminance  $E_v$  in lux. As stated in ref. [38] the most accurate way to determine the illuminance is to measure the absolute spectral irradiance and then calculate the illuminance. Unfortunately, most publications lack in absolute data and only provide the relative spectral irradiance of their LED,<sup>[14,15,17,21,25,26,33,63]</sup> which is much easier to obtain, in some cases not even relative light source spectra are given.<sup>[24,34,64]</sup> Hence, in many publications the illuminance is determined by a lux meter<sup>[15,16,21,25,29,30,32]</sup> and then the input power density is calculated with the measured illuminance and the relative spectra of the light source. The lux meter, however, only really measures relative photon densities and converts those to irradiance values using an assumption about the spectral shape of the light source. Typically, the assumption used is the so-called CIE standard illuminant A, that is, a black body with a temperature of 2856 K<sup>[65]</sup> which is similar to the spectrum of an incandescent light bulb but not to the spectrum of an LED.<sup>[66]</sup> While lux meters offer the option to use correction factors to account for different spectra of light sources, it is advisable to not rely entirely on a lux meter for the determination of illuminances and the correct calculation of an efficiency.<sup>[31,51,59,62,67]</sup>

Fortunately, if we want to know the spectral irradiance of an LED at a given illuminance (e.g., 200 lux), we can just calculate it, even if we only have the relative spectral irradiance at an arbitrary intensity. We know that, for example,

$$E_{v,200 \text{ lux}} : = 200 \text{ lux} : = \int E_{v,\lambda,200 \text{ lux}} d\lambda = f_{200 \text{ lux}} \int E_{v,\lambda,\text{ref}} d\lambda \quad (3)$$

where  $f_{200 \text{ lux}}$  is a factor that we have to multiply a known reference spectrum  $E_{v,\lambda,\text{ref}}$  with to obtain the spectral illuminance

$E_{v,\lambda,200 \text{ lux}} = f_{200 \text{ lux}} E_{v,\lambda,\text{ref}}$  at 200 lux. In Equation (3), we know all terms except  $f_{200 \text{ lux}}$  which we can therefore determine as

$$f_{200 \text{ lux}} = 200 \text{ lux} / \int E_{v,\lambda,\text{ref}} d\lambda \quad (4)$$

Initially, we do not know the integration kernel  $E_{v,\lambda,200 \text{ lux}}$  but we do know the result of the integral ( $E_{v,200 \text{ lux}} = 200 \text{ lux}$ ) and we assume that the LED spectrum does not change its shape, when the input power of the LED is changed to give different illuminances. Hence the desired information, namely,  $E_{v,\lambda,200 \text{ lux}}$ , follows as  $f_{200 \text{ lux}} E_{v,\lambda,\text{ref}}$ .

To correctly determine efficiencies, we need to accurately determine the input power density  $P_{\text{in}}(@200 \text{ lux})$  (irradiance) which can be calculated with the factor  $f_{200 \text{ lux}}$  and the measured relative spectral irradiance  $E_{e,\lambda,\text{ref}}$  via

$$P_{\text{in}}(@200 \text{ lux}) = E_e(@200 \text{ lux}) = f_{200 \text{ lux}} \int E_{e,\lambda,\text{ref}} d\lambda \quad (5)$$

Note that this calculation is exemplarily done for a set illuminance of 200 lux but can be performed for any illuminance, resulting in a set of factors  $f$  for different illuminances.

## 2.2. Adjusting the Output Power and Visualization of the Method

To illustrate the dependence of the input spectral irradiance  $E_{e,\lambda}$  of the used LED on the resulting efficiency, we discuss the effect of two exemplary LED light sources. The LEDs have the same color temperature of 2700 K according to manufacturer information but nevertheless have slightly different spectra. **Figure 2a** displays the spectral irradiance  $E_{e,\lambda}$  of the light source used in this work and of the light source used by Cui et al. in refs. [30,31]. Note that the spectral irradiances are already normalized to 200 lux as described above, which can be seen in the integral illuminance in **Figure 1b** (right y-axis). The LED used in this work exhibits an integral power density of  $77.85 \mu\text{W cm}^{-2}$  and the LED of Cui et al. has a power density of  $60.4 \mu\text{W cm}^{-2}$ . Although the LEDs are similar at first sight, the small shift of the LED peak of Cui et al., to lower wavelengths results in considerably different irradiances. The closer the LED peak is to the maximum of  $V(\lambda)$  at 555 nm, the more light usable to the human eye is in the spectra. As a consequence, smaller irradiances are needed to reach a certain constant illuminance. Thus, light sources with spectra close to  $V(\lambda)$  decrease the input power at constant illuminances.

The external quantum efficiency ( $Q_{e,\text{PV}}$ ) and the spectral irradiance are integrated over the wavelength to calculate the resulting short circuit current density

$$J_{\text{sc}} = \frac{q}{hc} \int Q_{e,\text{PV}} \times E_{e,\lambda} \times \lambda \times d\lambda \quad (6)$$

Here  $q$  is the elementary charge,  $h$  is Planck's constant, and  $c$  the speed of light. Equation (6) assumes that  $J_{\text{sc}}$  is linear with light intensity at the low light intensities relevant for indoor illumination and the similarly low light intensities that are typically present in a quantum efficiency measurement. If this condition of linearity is fulfilled, Equation (6) should provide a precise

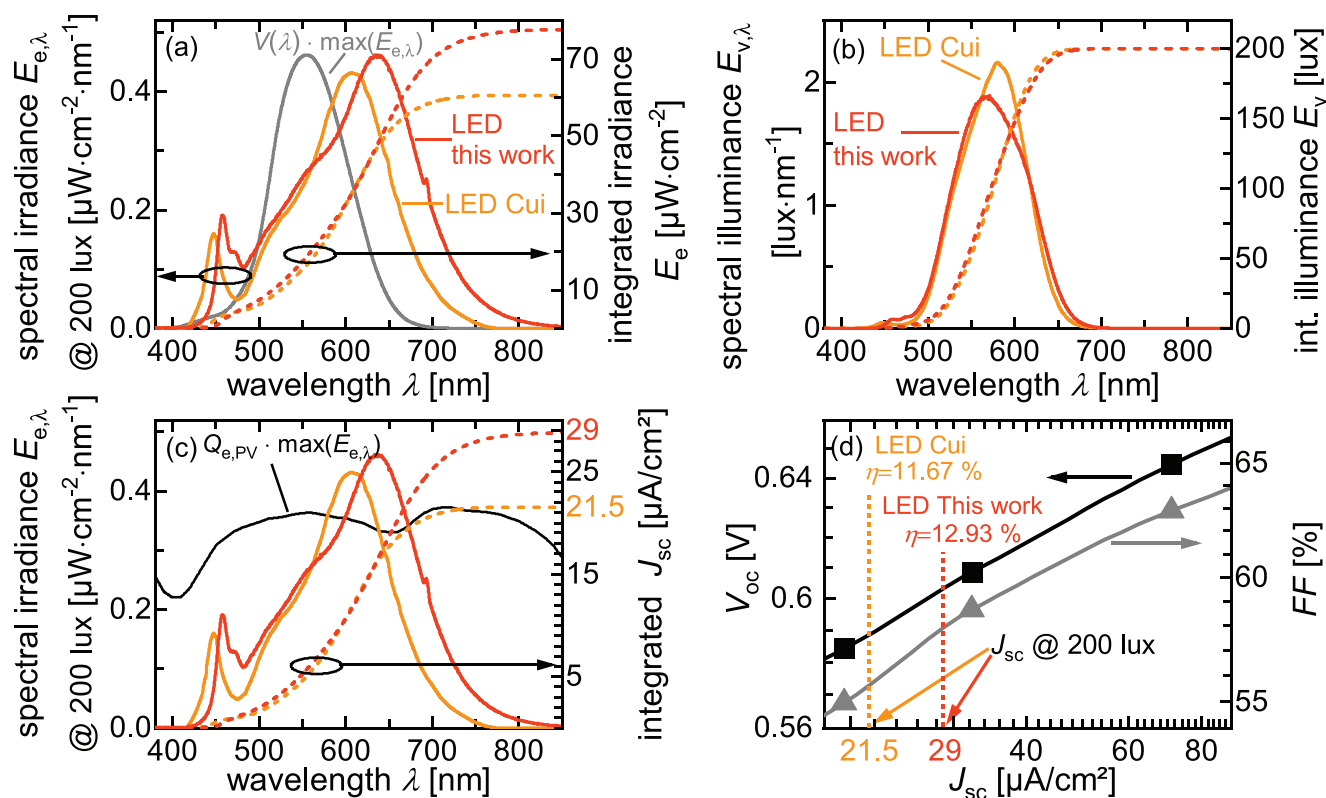


**Figure 2.** a) Relative spectral irradiance  $E_{e,\lambda}$  of two light sources with 2700 K normalized to 200 lux as described in Section 2.1. Red lines are the LED data used in this work and orange lines indicate LED data of refs. [30,31]. The accumulated integral irradiances are depicted as dashed lines on the right axis. By multiplication of the spectral irradiance with the luminous efficacy curve  $V(\lambda)$  the spectral illuminance in (b) is obtained. The integral illuminance (dashed lines) leads to the same value for both spectra due to the normalization of  $E_{e,\lambda}$  to 200 lux. c) The quantum efficiency  $Q_{e,PV}$  of a PBDB-TF-T1:Y12 sample is depicted, which is multiplied with the maximum spectral irradiance. The integration of the product of the  $Q_{e,PV}$  and the spectral irradiance  $E_{e,\lambda}$  gives the short circuit current density, which is shown with dashed lines accumulatively in (c) on the right axis (Equation (6)). d) The short circuit current densities are plotted on a double-logarithmic scale versus open-circuit voltages (squares) and fill factors (triangles), which were obtained by JV measurements. The lines exhibit interpolated values between the measured points. The output power of the solar cell at the specific illumination of 200 lux can be calculated by the  $J_{sc}$ , determined in (c) right axis, and the interpolated values of  $V_{oc}$  and  $FF$ . These interpolated values are emphasized with the orange and red dashed lines in (d). Finally, the efficiency at 200 lux can be determined from the exact input power and the output power of the solar cell.

value for  $J_{sc}$  under the spectral irradiance  $E_{e,\lambda}$ . When applying the proposed method to other solar cell technologies, care has to be taken that Equation (6) is still valid. In perovskite<sup>[68]</sup> as well as dye-sensitized solar cells,<sup>[69]</sup> deviations between the  $J_{sc}$  determined from Equation (6) and from solar simulator measurements have been reported in some cases. In organic solar cells, deviations between  $J_{sc}$  from Equation (6) and from solar simulator data have also been reported.<sup>[70]</sup> However, this typically only affects  $J_{sc}$  values measured at intensities around one sun and higher while there should be no non-linearities at the low light intensities relevant for indoor applications.<sup>[71,72]</sup>

Figure 2c, the quantum efficiency normalized to the maximal spectral irradiance and the resulting integrated short circuit current densities are shown for an organic solar cell with PBDB-TF-T1:BTP-4F-12 (PBDB-TF-T1:Y12) as the absorber material fabricated in our group, which was first shown in ref. [73]. The onset of the  $Q_{e,PV}$  is 872 nm and photovoltaic parameters at 1 sun illumination can be found in the Supporting Information. With the LED of Cui and co-workers a short circuit current density  $J_{sc}$  of  $21.5 \mu\text{A cm}^{-2}$  is obtained. With the slightly broader spectrum and the higher input power of the LED in our work, a

higher short circuit current density of  $28.8 \mu\text{A cm}^{-2}$  is reached. To determine the output power  $P_{out} = J_{sc} V_{oc} FF$  of the solar cell, JV characteristics at different light intensities close to the lux levels of interest are measured. The  $V_{oc}(J_{sc})$  and the  $FF(J_{sc})$  pairs are displayed in Figure 2d on a double logarithmic scale. By a pchip-interpolation (piecewise cubic hermite interpolating polynomial, see comment in Section 4) of  $V_{oc}(J_{sc})$  and  $FF(J_{sc})$  to the calculated  $J_{sc}$ ,  $P_{out}$  can be calculated for any given relative light source spectrum or illumination intensity. We assume that the open-circuit voltage and the fill factor are only dependent on the short circuit current density and not on the spectrum of the light source. With increasing photon energy, photons excite charge carriers to higher energy levels, which lose the excess energy by thermalization which eventually leads to the same  $V_{oc}$ . Measurements in refs. [31–33] (Table S7 in ref. [32] and Table 2 in ref. [31] and Table S1/Table S2 in ref. [33]) suggest that this assumption holds true and additional measurements can be found in Figure S1, Supporting Information.

As the  $J_{sc}$  increases for the LED in this work compared to the one for the LED of Cui and co-workers, the  $V_{oc}$  and the  $FF$  also shift to higher values. Consequently, the output power



increases from 7.0 to 10.1  $\mu\text{W cm}^{-2}$  for the LED of Cui et al. and the LED used in our work, respectively. Although the peak closer to 555 nm of the LED of Cui et al. boosts the efficiency with a lower input power as stated above, the efficiency is 11.67% compared to the LED of our work with 12.93%. For the LED of our work the gain of  $J_{\text{sc}}$  and therefore  $P_{\text{out}}$  due to the higher input power outweighs the efficiency loss due to the higher input power in the denominator, resulting in an absolute efficiency increase of 1.26%. The method presented above enables an in-depth analysis of the efficiency of organic solar cells under different light conditions. This example shows that apparently small differences in the spectral irradiance can have considerable effects on the resulting efficiency. First, a good overlap of the spectral irradiance and the luminous efficacy curve increases the efficiency at a given illuminance (i.e., 200 lux) due to lower input powers. Nevertheless, these lower input powers decrease the output power of the solar cell. Second, a maximized overlap of the samples' quantum efficiency and the spectral irradiances ensures a high  $J_{\text{sc}}$  and therefore a high output power. The interplay of these two effects can hardly be seen at first sight and makes the proposed analysis very valuable to find best performing combinations of light sources and absorber materials.

### 3. Results

#### 3.1. Verification of Method

To verify the method presented above, we apply the calculation to data of Cui and co-workers as they measured the spectral irradiance in absolute quantities with a calibrated spectrometer.<sup>[30]</sup> Cui et al. presented iOPV cells with PBDB-TF as donor and IT-4F, ITCC, and PC<sub>71</sub>BM as acceptor materials under illumination with a white LED with a color temperature of 2700 K.<sup>[30]</sup> Note that this is a relatively low color temperature for a white LED, that is, one with more photons in the red and less in the blue spectral region. The results are shown in **Figure 3** on a double-logarithmic scale. Filled symbols represent the original values of the three samples for illuminances of 200, 500, and 1000 lux as provided in ref. [30], whereas blank symbols show the results of our calculation. First, we address the normalization of the spectral irradiance to the applied lux levels. The integration according to Equations (1) and (2) gives a  $E_{\text{v,ref}}$  of 46425.97 lux which leads to normalization factors of 0.0043, 0.0108, and 0.02154 for the  $E_{\text{v,set}}$  of 200, 500, and 1000 lux, respectively. Note that we apply the calculation to relative spectral irradiance data, although absolute measurements are available in order to prove the applicability to relative data. The integration of the factorized reference spectra  $f \cdot E_{\text{e},\lambda,\text{ref}}$  results in input power densities of 60.38, 150.96, and 301.91  $\mu\text{W cm}^{-2}$  for 200, 500, and 1000 lux, respectively. The input power densities are shown in Figure 3a and match well with the original absolute data. The integration according to Equation (6) gives  $J_{\text{sc}}$  values, which are in good agreement with the original  $J_{\text{sc}}$  values of Cui and co-workers as well and are depicted in Figure 3b. Only the PBDB-TF:PC<sub>71</sub>BM cell shows a slight deviation with a calculated  $J_{\text{sc}}$  of 18.63  $\mu\text{A cm}^{-2}$  to the original value of 18.9  $\mu\text{A cm}^{-2}$ , which is likely to originate from

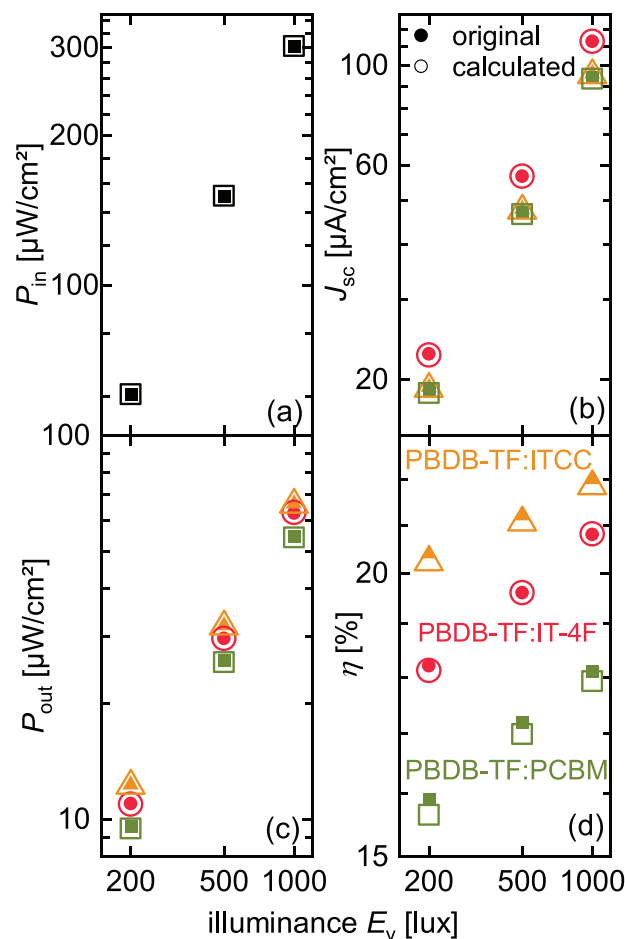


**Figure 3.** Comparison of original data of Cui et al., from ref. [30] (filled symbols) and our calculation (blank symbols) on a double-logarithmic scale. Illuminance dependent data of a)  $P_{\text{in}}$ , b)  $J_{\text{sc}}$ , c)  $P_{\text{out}}$ , and d) the efficiency  $\eta$  are shown. The overlap of filled and blank symbols proves the correctness of the performed calculation.

slight discrepancies in the  $J_{\text{sc}}$  from the JV measurement and the  $J_{\text{sc}}$  from  $Q_{\text{e,pv}}$ . As the  $V_{\text{oc}}$  and  $FF$  are computed by interpolation, a well matching  $J_{\text{sc}}$  automatically results in a good match of the values for  $V_{\text{oc}}$  and  $FF$ , which can be seen in Figure S2, Supporting Information. Figure 3c,d shows the resulting output power densities and efficiencies. Apart from a slight deviation of the PBDB-TF:PC<sub>71</sub>BM sample due to the  $J_{\text{sc}}$  difference, the calculated output power densities and efficiencies are in excellent agreement with the original data.

In the Supporting Information a detailed analysis of a range of published data is shown (Figures S3–S9, Supporting Information), where the necessary data was available. In about 65% of the studied data the efficiency stated in the publication and calculated with our method are in good agreement, which means deviation is only about 1% (in total). In the other 35% of the evaluated data the stated and the measured absolute efficiency is deviating >3% in total, in worst cases > 8% in total, which emphasizes the need of establishing low light measuring protocols. The deviations can have the following reasons: First, inconsistencies in the theoretical input powers (calculated with the relative LED spectra normalized to 200 lux) and the given

input powers in the references imply that the illumination is not measured precisely. Therefore, the performance parameters are measured at an arbitrary point of illumination. If the lux meter for instance underestimated the illumination and the measured points would be on a slightly higher illuminance in reality, this error propagates to all performance parameters. Consequently, the  $J_{sc}$  of the apparent 200 lux would seem higher, because in reality it might have been measured at say 210 lux. A detailed discussion can be found in the Supporting Information. Second, as stated in ref. [59], the theoretical  $J_{sc}$  ( $J_{cal}$  in the ref. [59]) should be consistent with the  $JV$  measurement, which is not the case for many publications. This inconsistency indicates that either the  $Q_{e,PV}$  or the LED spectra are of insufficient accuracy. Consequently, an overlap of calculated data points and original data cannot be achieved, because our calculation is based on the integrated  $J_{sc}$  from the quantum efficiency whereas most publications work with the  $JV$  measurement data. Additionally, we remark to check the correct calculation of the efficiency, because in some data the simple equation  $\eta = J_{sc} V_{oc} FF / P_{in}$  does not hold true or it is not clear from which parameters the efficiency is calculated. If all data is measured precisely at a defined illumination, theoretical values and the original data must match well. Therefore, this method also gives the chance to validate low light measurements and editors or reviewers can judge whether some data credibly reports a certain efficiency under a certain illumination condition. Note that optical neutral density (ND) filters, which may be used to achieve sufficiently low light intensities, have (unlike what the name suggests) a wavelength-dependent transmission which varies mostly at the edge of the visible spectrum. Thus, in particular the region  $\lambda > 700$  nm becomes problematic, because at these wavelengths many organic solar cells for indoor applications will still absorb light well. The spectral dependencies of ND filters will cause changes in the spectra if used in low light set-ups and will therefore affect  $P_{out}$  but more importantly  $P_{in}$  at 200 lux and the efficiency.

As there are inconsistencies for a huge amount of publications, this emphasizes the need of a reliable comparison method. Even if the concept of efficiencies would be omitted to circumvent the determination of the input power, the output power is heavily dependent on the illumination. The output power may be measured correctly, but if the illumination is wrongly determined the comparison of publications is impossible due to the shift of the lux axis. Therefore, we strongly recommend the comparison with calculated values based on the spectra and the quantum efficiency as this method does not only verify the measured values, but also enables a high level of comparability between different labs, setups, and light sources.

### 3.2. Influence of LEDs with Different Photon Energies on the Performance of Indoor Solar Cells

Publications use different LEDs with varying photon energies to examine the performance of iPVs. Different photon energies affect the efficiency of solar cells by the direct influence on the input power. Furthermore, the solar cells'  $Q_{e,PV}$  onset should be suitable for a certain type of LED, so that an

optimal absorption of the incoming light over all wavelengths is ensured.

First, we discuss the case for perfect absorption by applying a modified version of the Shockley–Queisser<sup>[74]</sup> model based on the principal of detailed balance<sup>[75]</sup> to different LED spectra. Freunek et al., had previously presented a calculation for different types of light sources, but at a constant irradiance<sup>[76]</sup> and Ho et al., had presented calculations which mainly focused on the influence of different illuminances.<sup>[77]</sup> Similar calculations were performed for other technologies<sup>[52]</sup> or used empirical approaches.<sup>[78–80]</sup> Here, in contrast to Freunek et al., we examine the influence of different LED light sources at constant illuminance instead of the constant irradiance calculation done by Freunek et al. The detailed balance model assumes a single abrupt absorption onset, that is, in mathematical terms a step-function like absorptance of the absorber layer that is zero below the band gap and one above the band gap. This idealization is a sensible upper limit for efficiency and different solar cell technologies come differently close to an abrupt absorption onset. Early generations of organic solar cells featured substantial losses<sup>[81,82]</sup> due to non-abrupt absorption onsets caused by the different absorption feature of the donor, the acceptor, and the charge transfer state. Therefore, variants of the detailed balance model with Gaussian,<sup>[83]</sup> exponential,<sup>[84]</sup> or multistep-absorption onsets<sup>[85]</sup> were devised. The efficiency improvements in recent generations of organic solar cells have however led to substantially steeper absorption onsets<sup>[86,87]</sup> and smaller differences between donor, acceptor, and CT state absorption features.<sup>[88,89]</sup> These developments imply that the original Shockley–Queisser model becomes more relevant with the continuous improvement of OPV efficiencies and motivates our use of the traditional step-function. In addition to the step-function absorptance, the detailed balance model also idealizes the contacts (no resistive losses), transport (all photogenerated electron hole pairs are collected), and recombination (only radiative recombination is included in the model). In reality, losses will occur due to imperfect contacts, finite mobilities, and due to non-radiative recombination and thereby lead to lower than optimum efficiencies. A detailed description of the performed calculation can be found in the Supporting Information.

In Figure 4a the spectra of LEDs with different photon energies are depicted, which were normalized to 200 lux as described above. The LED of Ding et al., shows the highest photon energies with a main peak at  $\approx 450$  nm. As the LEDs decrease in color temperature, the main peak decreases and the other peak gets more pronounced. The LED with 2700 K used in our group exhibit the lowest photon energies and shows a main peak around  $\approx 640$  nm. Note that the color temperatures given by the manufacturer are insufficient to characterize the spectra. We found different color temperatures (stated by the manufacturer) for similar spectra in literature as well as identical color temperatures for different spectra. In Figure 4b the integrated irradiances are shown. The values at 800 nm are the input power densities of the LED. At a constant illuminance, LEDs with spectra close to the  $V(\lambda)$  maximum at 555 nm (such as the 4100 K LED) need less input power for a certain illuminance. Consequently,  $P_{in}$  is decreasing from LEDs with high photon energies to the 4100 K LED as the spectra shift closer to the  $V(\lambda)$  maximum. Subsequently,  $P_{in}$  increases for the 2700 K

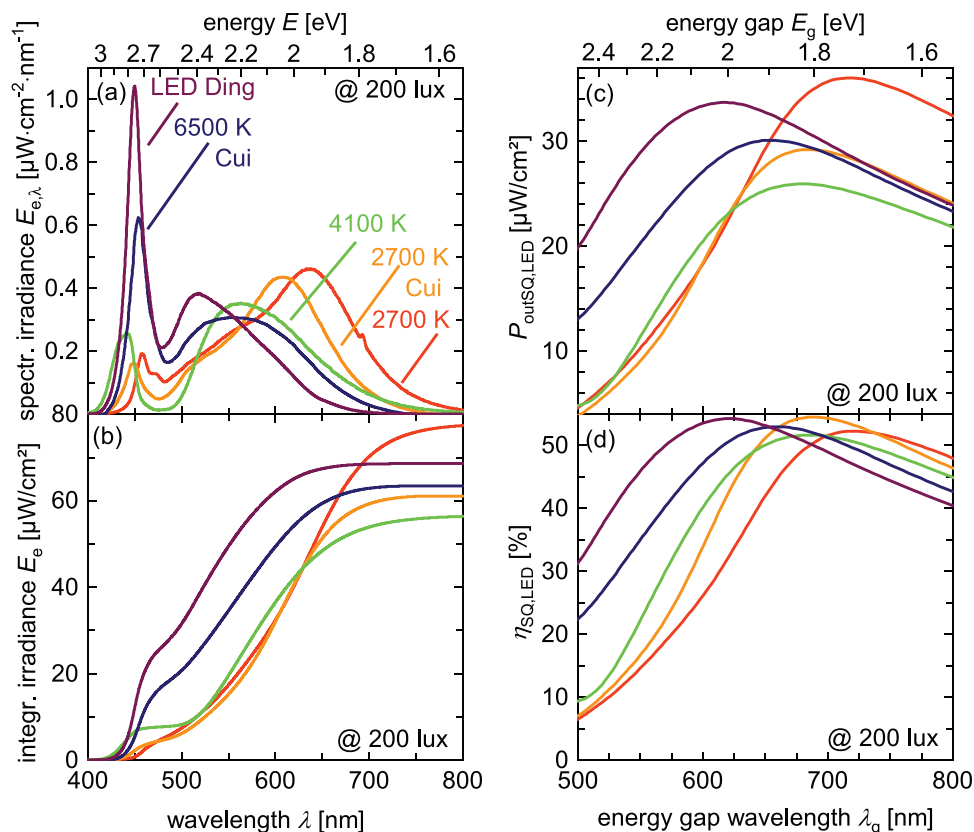


**Figure 4.** a) Spectral irradiance and b) integrated irradiance data for a selection of LEDs (LED Ding from ref. [33], LED 6500 K, and LED 2700 K from ref. [30] and LED 4100 K and 2700 K are from our group). The spectra were normalized to 200 lux as described above. For the input spectra c) the output power  $P_{\text{out,SQ,LED}}$  and d) the efficiency  $\eta_{\text{SQ,LED}}$  within the adapted Shockley–Queisser model were calculated. The maximum output power is following the input power as all LED spectra were normalized to a constant illuminance of 200 lux.

LED of Cui et al. and the 2700 K LED of our group as more input power is needed to reach the constant illuminance of 200 lux.

With the spectra normalized to 200 lux, the performance parameters were calculated within the Shockley–Queisser model. In Figure 4c,d the resulting output power densities  $P_{\text{out,SQ,LED}}$  and the efficiency  $\eta_{\text{SQ,LED}}$  are depicted, respectively. All other performance parameters can be found in Figure S10, Supporting Information. For the LED of Ding et al., the maximum  $P_{\text{out,SQ,LED}}$  of  $33 \mu\text{W cm}^{-2}$  is found for materials with a band gap of 2 eV. With decreasing LED photon energies, the maximum  $P_{\text{out,SQ,LED}}$  is decreasing as the input power is decreasing. The maximum output power of the LED with 4100 K is shifted to band gaps of 1.8 eV and amounts to  $26 \mu\text{W cm}^{-2}$ . Subsequently, with decreasing photon energies the  $P_{\text{out,SQ,LED}}$  is increasing again and reaches its maximum of  $36 \mu\text{W cm}^{-2}$  for the 2700 K LED with a band gap of 1.7 eV. Hence, the maximum output power is strongly affected by the spectrum of the LED. Spectra close to the  $V(\lambda)$  maximum of 555 nm have lower output powers for the situation of constant illuminances. As we pointed out in Section 2.2, the spectra of different LED have a strong influence on the efficiency of the solar cell. Our calculations are done with different LED spectra compared to the existing ones in literature, implying that we will not get identical but only similar results. For instance,

the spectrum of the 2700 K LED of Cui et al.<sup>[30]</sup> resembles the 3000 K LED spectrum of Ho et al.<sup>[77]</sup> (Table S1(b) in ref. [77]) and hence leads to similar efficiency values in the modified SQ model. Ho et al. state an input power of  $59.6 \mu\text{W cm}^{-2}$  at 200 lux with an optimal absorber band gap of 1.83 eV and a maximum efficiency of 53.24%, which are in good agreement with our results (input power of  $60.7 \mu\text{W cm}^{-2}$ , optimal absorber band gap of 1.80 eV, and a maximum efficiency of 54.4%). The results of other LEDs used by Ho et al. differ slightly due to slightly different input spectra.

To investigate the effect of LED spectra on actual organic solar cells, a selection of well-performing solar cells with different absorption band onsets were investigated. Note, that although in this study we focus on OPV, our method is applicable to all solar cell technologies. The  $Q_{\text{e,PV}}$  of the solar cells can be found in Figure S11, Supporting Information, and the wavelength of the band gap  $\lambda_g$  was determined by finding the inflection point of the  $Q_{\text{e,PV}}$  data.<sup>[90]</sup> The values of  $\lambda_g$  are 644, 675, 702, and 803 nm for the CD1:PBN-10 (Ding et al., ref. [33]), PBDB-TF:IO-4Cl (Cui et al., ref. [31]), PBDB-TF:ITCC (Cui et al., ref. [30]), and the PM6:Y6-O (Ma et al., ref. [35]) solar cell, respectively. As the  $\lambda_g$  is increasing, the color code in Figure 5 changes from orange to brown. High band gap samples typically reach lower short circuit current densities and higher open-circuit voltages than lower band gap solar cells, and vice

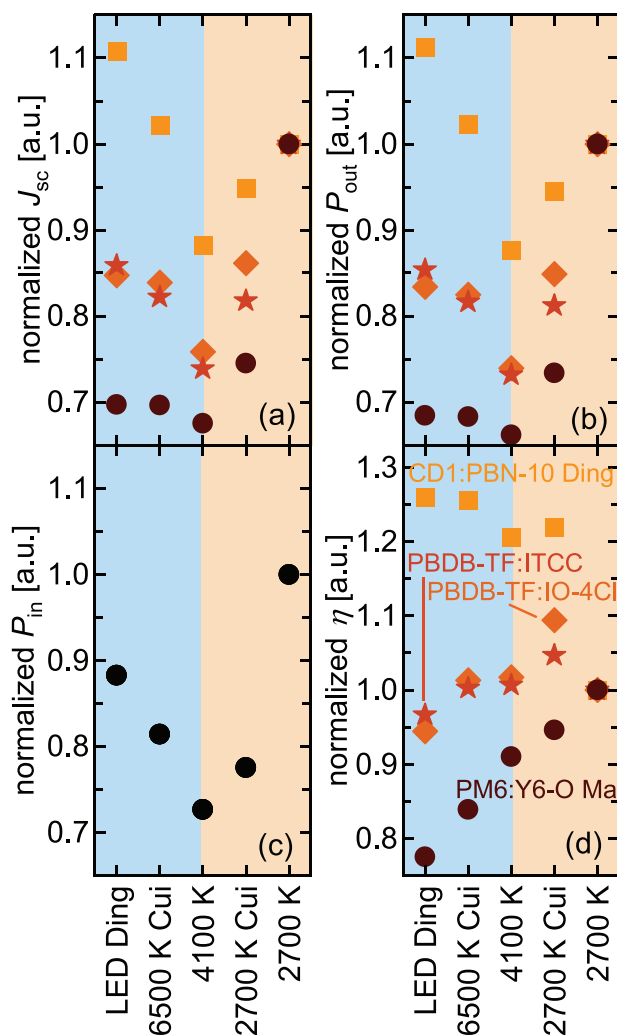


**Figure 5.** Performance parameters of highly efficient solar cells with varying onset  $\lambda_g$  of the quantum efficiency  $Q_{e,pv}$  performing under different LED light sources with constant illumination of 200 lux. The colors change from orange to brown for samples with increasing  $\lambda_g$  of the  $Q_{e,pv}$ . The a)  $J_{sc}$ , b) the  $P_{out}$ , c) the  $P_{in}$ , and d) the  $\eta$  were normalized to the results of the 2700 K LED with lowest photon energies. Samples with high band gaps (low  $\lambda_g$ , orange symbols) are better performing with high color temperature LEDs and samples with low band gaps (higher  $\lambda_g$ , brown symbols) excel for LEDs with lower color temperature. Note, that due to the normalization to the LED with 2700 K all points overlay for the LED with 2700 K.

versa for low band gap materials. For each LED spectrum, there is an optimal band gap that minimizes losses in  $J_{sc}$  (i.e., non-absorption losses) and  $V_{oc}$  (i.e., thermalization and recombination losses) such that we achieve the maximum efficiency. As this influence shifts the absolute efficiency, all parameters and the input power of the LEDs shown in Figure 5 were normalized to the values of the LED with 2700 K. Hence, we can investigate the relative influence of different LED spectra on the performance parameters. The x-axis of Figure 5 is sorted from LEDs with high to low color temperature from left to right (i.e., cold white to warm white). The first (second) region with higher (lower) photon energy LEDs is marked with blue (red) rectangles as guide to the eye. Absolute values as well as the

$V_{oc}$  and  $FF$  dependence are displayed in Figure S12, Supporting Information.

Figure 5 shows the normalized  $J_{sc}$ ,  $P_{out}$ ,  $P_{in}$ , and  $\eta$ , respectively. All four parameters vary by about 15% to 25% due to the different overlap of the LED spectra with the eye sensitivity and the solar cell quantum efficiencies. Depending on the absorber material, the efficiency may increase (e.g., low band gap material PM6:Y6-O) or decrease (e.g., high band gap material CD1:PBN-10) with decreasing color temperature, indicating that low band gap materials perform better with low color temperature LEDs and vice versa (Figure 4d). The color temperature dependence of the efficiency implies that any ranking or comparison of indoor solar cells strongly depends on the used LED.

We conclude, that the performance of iPV depends on the delicate interplay between the spectral irradiance of the LED and the quantum efficiency  $Q_{e,pv}$  of the solar cell. LEDs with spectra close to the luminous efficacy curve exhibit lower input powers, which decrease the output power. The efficiency dependence on the LEDs color temperature is changing with the band gap of the absorber material. For high band gaps, a high color temperature LED is more suitable and for materials with low band gaps, a LED with low color temperature is performing better.

### 3.3. Comparing Efficiencies of Different Publications

Comparing efficiencies of different publications is hard to handle fairly due to the variety of light sources and used illumination intensities. This problem is widely known and discussed in literature<sup>[31,51,59,62,91]</sup> and studies of Cui et al. depicted origins of measuring errors and developed measuring protocols. Nevertheless, the problem of comparing data generated with different light source spectra still remains. With our presented method we can rank photovoltaic cells across literature for the first time, although the original data was measured under one specific light source. In the following this is exemplarily shown for OPV technology.

As we have seen above, different LED spectra favor different blends with varying absorption onsets thereby complicating any fair comparison between literature data. Thus, we propose to compare and rank efficiencies and output powers at 200 lux by choosing the best LED for each solar cell. The “best” LED means the one which leads to the highest efficiency under an illuminance of 200 lux.

First, the calculation was carried out for a wide set of data from literature<sup>[16–19,30–35]</sup> for the whole set of different LEDs presented above with a constant illuminance of 200 lux. Unfortunately, some high-performance solar cells could not be included due to lack of necessary data. To get an overview, only the performance parameters for each sample resulting from the LED irradiation with the best efficiency are considered. The threshold efficiency for inclusion in the study was 10% at 200 lux under at least one of the 5 LED spectra shown in Figure 4a. In Figure 6 the performance parameters are plotted against the publications with increasing efficiency. All samples which reached the best efficiency with the LED of Ding et al., the LED with 2700 K of Cui et al. and the LED with 2700 K used



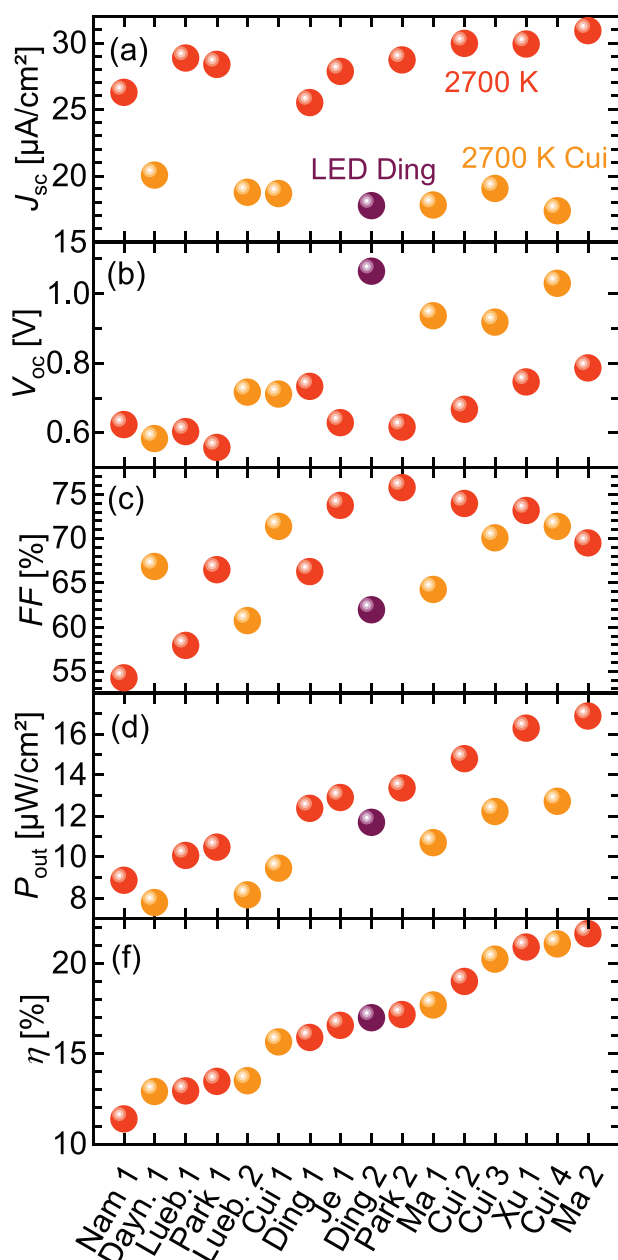


**Figure 6.** Performance parameters of the analyzed samples are displayed and sorted by increasing efficiency on the x-axis. To rank the efficiencies, the calculation was done for the whole set of five LEDs, but only the highest resulting efficiency is shown. Efficiencies resulting from illumination with the LED of Ding et al., the LED with 2700 K of Cui et al., and the LED with 2700 K used in our work, are displayed in purple, orange, and red color, respectively. Materials of one publication are numbered and the specific material of the respective publication can be found in Table S1, Supporting Information.

in our work, are displayed in purple, orange, and red color, respectively. In Tables S1 and S2, Supporting Information, the parameters are listed and the materials and references can be found as well.

This comparison also includes two absorber blends fabricated in our group. The high band gap blend PBDB-T:F-M and the low band gap blend PBDB-TF-Tl:Y12 are fabricated with the

green solvent *o*-xylol and the 0.16 cm<sup>2</sup> devices exhibit an active layer area thickness of around 190 and 180 nm, respectively, which is higher than optimal for 1 sun performance. For the PBDB-T:F-M device the performance under 1 sun illumination was relatively poor with a  $J_{sc}$  of 12.4 mA cm<sup>-2</sup>, a  $V_{oc}$  of 0.89 V and a  $FF$  of 49.9%, leading to an efficiency of 5.5%. With an efficiency of 12.2%, the PBDB-TF-Tl:Y12 device strongly outperformed the PBDB-T:F-M solar cell under 1 sun illumination with a  $J_{sc}$  of 24.4 mA cm<sup>-2</sup>, a  $V_{oc}$  of 0.84 V and a  $FF$  of 59.5%. All  $JV$  and  $Q_{e,pv}$  measurements can be found in Figure S13, Supporting Information, and performance parameters for 1 sun and low light illumination are listed in Tables S3 and S4, Supporting Information. Figure 6 illustrates, that under an illumination of 200 lux the PBDB-T:F-M (2700 K LED, Lueb. 2. in Figure 6) and the device PBDB-TF-Tl:Y12 (2700 K LED Cui, Lueb. 1 in Figure 6) reach efficiencies of 13.5% and 12.9%. This example manifests, that devices, which perform poorly under for 1 sun conditions, can be well performing in the low light regime.

In Figure 7 the performance parameters are plotted against the band gap wavelength  $\lambda_g$ . In accordance to the Shockley–Queisser model, materials with lower band gaps exhibit higher short circuit current densities  $J_{sc}$  and lower open-circuit voltage  $V_{oc}$ . The efficiency peaks around band gap wavelengths of  $\approx 675$  nm ( $\approx 1.84$  eV) for the illumination with the 2700 K LED of Cui et al. The maximum for the illumination with the 2700 K LED used in our group is located around a band gap wavelength of  $\approx 800$  nm ( $\approx 1.55$  eV).

To illustrate if these maxima are in accordance to the Shockley–Queisser calculation, in Figure 8 the efficiencies of our meta-analysis as well as the maximum efficiencies from the Shockley–Queisser calculation are plotted. Straight lines exhibit the maximum Shockley–Queisser efficiencies for the different input LED spectra. Dashed lines incorporate an additional, non-radiative voltage loss of 180 meV representative of the lowest reported values in the literature that are in the range of 0.16–0.2 V.<sup>[88,92,93]</sup>

For the samples, which reached the best efficiencies with the 2700 K LED of Cui et al., the peak around 1.84 eV is overlapping with the position of the Shockley–Queisser maximum, suggesting the band gap to be suitable for this LED illumination. Theoretically, with this kind of LED spectrum a maximum efficiency of 54% is possible, emphasizing the potential for further improvements. Interestingly, the best experimental efficiencies for the 2700 K LED at 1.55 eV (red symbols compared to red line) do not coincide with the Shockley–Queisser maximum of 1.7 eV. This could imply that the electronic quality of the materials dominates the optimum band gap for the experimental data. All in all, this detailed analysis manifests the state of the art for iOPV and shows that there is still substantial room for improvement for all three PV parameters ( $J_{sc}$ ,  $V_{oc}$ , and  $FF$ ).

## 4. Conclusion

In this work, we proposed a method, which enables the calculation of efficiencies at a fixed illumination level based on simple standard measurements as  $JV$  and quantum efficiency

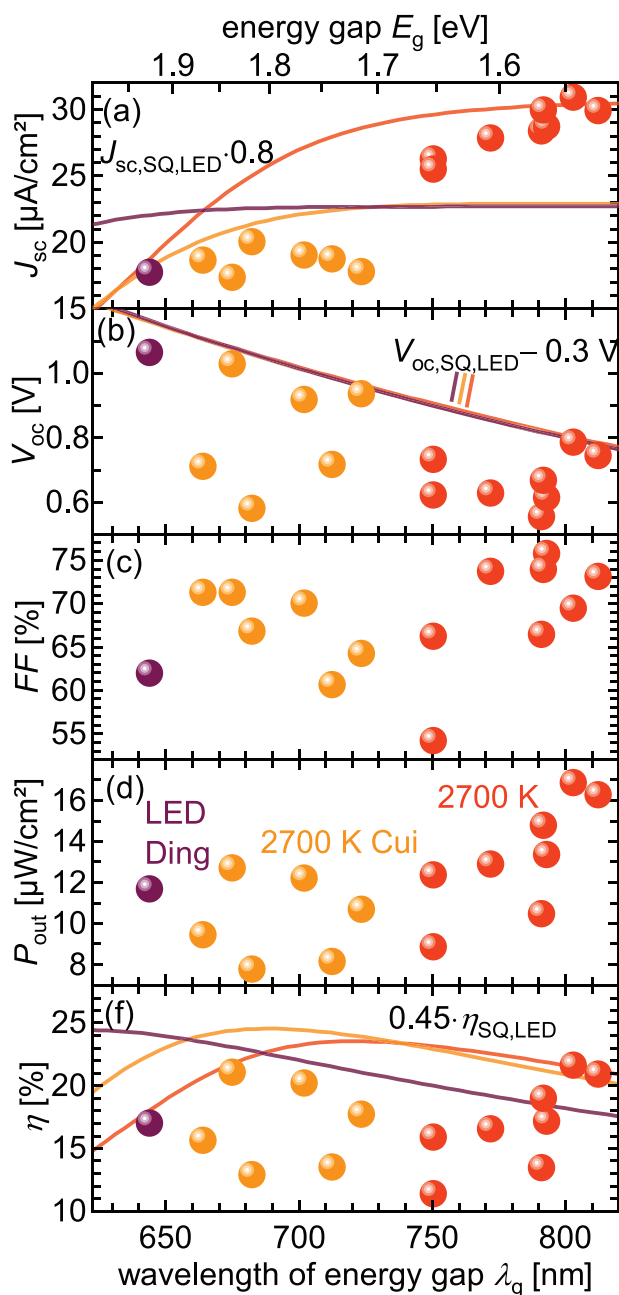


**Figure 7.** Performance parameters of a wide range of samples from literature plotted against the wavelength of the band gap. Specific information about the materials and publications can be found in Table S2, Supporting Information. Straight lines with colors of the respective LED light source are shown to indicate the trends of the maximum performance (modified Shockley–Queisser model). Note, that the lines are adjusted with arbitrary constants to better fit the experimental data, so that the lines fulfill their purpose as guide to the eye. The  $J_{sc}$  was adjusted to 80% of the maximum  $J_{sc}$  and the efficiency to 45% of its maximum. Furthermore, we subtracted 0.3 V from the maximum  $V_{oc}$  to better match the values. Note that the  $V_{oc}$  lines for the different LEDs overlap as they only depend weakly on the used LED source.

measurements. The possibility to scan the performance for different LED emission spectra and light intensities, ensures a fair comparison between PV publications as the arbitrariness

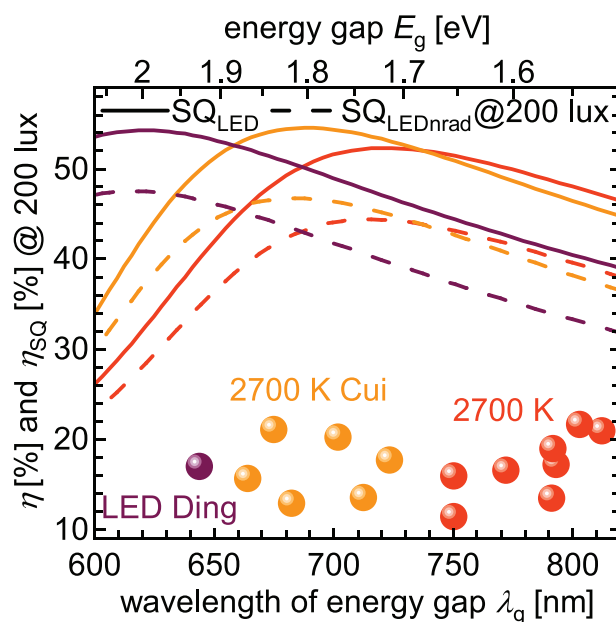


**Figure 8.** Efficiencies resulting from our calculations for a constant illuminance of 200 lux for a wide set of iOPV devices from literature (dots). Straight lines show the Shockley-Queisser efficiencies resulting from illumination of the LED of Ding et al. (purple), the 2700 K LED of Cui et al. (orange), and the 2700 K LED used in our group (red). Efficiencies resulting from Shockley-Queisser calculations with a non-radiative voltage loss of 180 meV are depicted in dashed lines.

of low light setups is inevitable. While our method is applicable to any solar cell technology, where  $J_{sc}$  can be precisely determined from the external quantum efficiency, we apply our method to organic solar cells whose data are either measured in house or taken from literature. First, we validated our evaluation method thoroughly and showed that about 65% of the efficiencies studied from literature are in good agreement with our model. The other 35% showed total deviations of the absolute efficiency  $>3\%$ , including some absolute efficiencies deviating  $\approx 8\%$ . These deviations stress the need for consistency checks of low light efficiencies using quantum efficiency data and LED spectra to support the current voltage curves. Furthermore, we demonstrated quantitatively the delicate dependence of the output power and the efficiency of iOPVs on the LED spectra. The efficiencies are governed by the overlap of the quantum efficiency and the LED spectrum and vary by  $\pm 20$ – $25\%$  when using different LED spectra depending on the absorber band gap. Calculations with an ideal absorber within the Shockley–Queisser limit with a fixed illumination of 200 lux completed this study and emphasized that there is still substantial room for improvement of this technology as the maximum Shockley–Queisser efficiency is 52–54% depending on the used LED spectrum. The optimal band gap of the absorber depends on the LEDs' spectrum and is ranging between 1.75 and 2 eV. Finally, we analyzed a wide set of different iOPVs from literature and rank them according to their efficiency under the LED that fits each cell best. This fair comparison shows that the presented calculation is a powerful tool to detect possible candidates for high indoor performance solar cells for an arbitrary light source.

## 5. Experimental Section

**Stepwise Calculation of  $\eta$ :** In the first step the input power of the light source was determined (Section 2.1). The relative spectral irradiance  $E_{e,\lambda,\text{ref}}$  data was supposed to be in units of  $\text{W}/\text{m}^2/\text{nm}$  and could be measured by a spectrometer. The spectral illuminance  $E_{v,\lambda,\text{ref}}$  was calculated by Equation (2). Integration of the relative spectral irradiance  $E_{e,\lambda,\text{ref}}$  and the spectral illuminance  $E_{v,\lambda,\text{ref}}$  lead to the reference irradiance  $E_{e,\text{ref}}$  and the reference illuminance  $E_{v,\text{ref}}$ . Then, the factor  $f$  for a certain illuminance (e.g., 200 lux) was calculated with  $f_{200 \text{ lux}} = 200 \text{ lux}/E_{v,\text{ref}}$  (Equation (4)), leading to one factor for each illuminance level. The irradiance at the chosen illuminance level could be calculated with  $P_{\text{in}} = f_{200 \text{ lux}} E_{e,\text{ref}}$  (Equation (5)). After multiplying  $E_{e,\lambda,\text{ref}}$  with the factor  $f_{200 \text{ lux}}$ , the relative spectral irradiance data was normalized to the desired illuminance and the determination of the light sources' input power was done.

In the second step the output power of the solar cell was adjusted (Section 2.2). The short circuit current density was calculated by Equation (6), using the normalized spectral irradiance data. The  $V_{\text{oc}}(J_{\text{sc}})$  and  $FF(J_{\text{sc}})$  data was gained by JV measurements close to the desired lux levels with any light source. Then, the exact  $V_{\text{oc}}$  and  $FF$  values were determined by a "pchip" interpolation. Linear interpolation should obtain similar results, but the "pchip" interpolation proved to match better results in case of considering whole ranges of illuminance levels (from 200 to  $10^5$  lux) or in case of extrapolation to smaller  $J_{\text{sc}}$  (calculated  $J_{\text{sc}}$  from  $Q_{\text{e,pv}}$  smaller than measured  $J_{\text{sc}}$  from JV). Now  $P_{\text{out}} = J_{\text{sc}} V_{\text{oc}} FF$  gave the output power and with the input power of Section 2.1 the efficiency could be calculated. The Matlab code can be found on [https://github.com/tkirchartz/Determine\\_Indoor\\_PV\\_Performance](https://github.com/tkirchartz/Determine_Indoor_PV_Performance).

**Device Fabrication:** First, a structured indium tin oxide (ITO) layer ( $\approx 150$  nm) on glass was cleaned in an ultrasonic cleaner for 10 min in distilled water, acetone and isopropyl alcohol, respectively. The substrates were dried at  $100^\circ\text{C}$  on a hotplate and treated with an oxygen plasma. For the PBDB-T:F-M samples the device structure was ITO/ZnO/blend/MoO<sub>x</sub>/Ag and for the PBDB-TF-T1:BTP-4F-12 (PBDB-TF-T1:Y12) samples the device structure was ITO/PEDOT:PSS/blend/PFN-Br/Ag.

For the PBDB-T:F-M devices, the zinc oxide (ZnO) interlayer was processed from a sol-gel. 100 mg of zinc acetate dihydrate (Sigma Aldrich), 1.5 mL 2-methoxyethanol (Alfa Aesar) and 28  $\mu\text{L}$  ethanol amine (Sigma Aldrich) were stirred at  $60^\circ\text{C}$  overnight and filtered with a  $0.45 \mu\text{m}$  PVDF filter. The ZnO sol-gel was spin-coated on top of the ITO with 6000 rpm for 50 s and was annealed at  $200^\circ\text{C}$  for 20 min, resulting in a ZnO layer of  $\approx 30$  nm. The devices were transferred into a glovebox for further preparation.

The polymer **PBDB-T** poly[[4,8-bis[5-(2-ethylhexyl)-2-thienyl]benzo[1,2-b:4,5-b']dithiophene-2,6-diyl]-2,5-thiophenediyl[5,7-bis(2-ethylhexyl)-4,8-dioxo-4H,8H-benzo[1,2-c:4,5-c']dithiophene-1,3-diyl]] and the NFA **F-M** 4,4,7,7,12,12-octyl-7,12-dihydro-bis [ethylidene(3-oxomethyl-1H-indene-2,1(3H)-diylidene)]bis-4H-thieno[2'',3'':1',2']indeno[5',6':5,6]-s-indaceno[1,2-b]thiophenein were purchased from 1-material. PBDB-T and F-M were dissolved with a 1:1 ratio and a concentration of  $17 \text{ mg mL}^{-1}$  in ortho-xylene (o-xylene). The solution was stirred overnight at  $100^\circ\text{C}$  in the glovebox and prior to spin-coating 0.2% of 1,8-dioctane (DIO) was added. The solution was spin-coated dynamically with a speed of 1000 and 3000 rpm for 40 s to obtain an active layer with thicknesses of  $\approx 190$  nm and  $\approx 100$  nm, respectively. Thicknesses were estimated with capacitance measurements as described below. Finally, 8 nm of MoO<sub>x</sub> and  $\approx 100$  nm silver (Ag) were evaporated under high vacuum ( $\approx 5 \times 10^{-7}$  mbar). The device area was defined by a shadow mask and was  $0.16 \text{ cm}^2$  for devices for 1 sun JV and  $Q_{\text{e}}$  measurements and  $0.06 \text{ cm}^2$  for devices for measurements of  $V_{\text{oc}}(J_{\text{sc}})$  and  $FF(J_{\text{sc}})$  pairs in the low light regime.

For the PBDB-TF-T1:Y12 samples, poly(3,4-ethylenedioxythiophene) polystyrene sulfonate PEDOT:PSS Al 4083 from Ossila was treated with an ultrasonic cleaner under cooling for 15 min before filtering with a  $0.45 \mu\text{m}$  PVDF filter. The PEDOT:PSS was spin-coated at 4000 rpm for 30 s and then annealed at  $150^\circ\text{C}$  for 20 min. The substrates were subsequently transferred into a nitrogen atmosphere. For the active

layer, the donor **PBDB-TF-T1** Poly[(2,6-(4,8-bis(5-(2-ethylhexyl-3-fluoro)thiophen-2-yl)-benzo[1,2-b:4,5-b']dithiophene))-alt-(5,5-(1',3'-di-2-thienyl-5',7'-bis(2-ethylhexyl)benzo[1',2'-c:4',5'-'] dithiophene-4,8-dione))-ran-poly[(2,6-(4,8-bis(5-(2-ethylhexyl)thiophen-2-yl)-benzo[1,2-b:4,5-b']dithiophene))-alt-(2,2-ethyl-3(or4)-carboxylate-thiophene)] and the NFA **BTP-4F-12** 2,2''-((2Z,2''Z)-((12,13-bis(2-butyloctyl)-3,9-diundecyl-12,13-dihydro-[1,2,5] thiadiazolo[3,4-e]thieno[2'',3'':4',5'']thieno[2'',3'':4,5] pyrrolo[3,2-g]thieno[2'',3'':4,5]thieno[3,2-b]indole-2,10-diyl) bis(methanylylidene))bis(5,6-difluoro-3-oxo-2,3-dihydro-1H-indene-2,1-diylidene)) dimalononitrile (Y12) (purchased from 1-material) were dissolved with a ratio 1:1.2 in o-xylene with a concentration of  $25 \text{ mg mL}^{-1}$  and stirred at room temperature about 3 h before spin-casting. The solution was spin-coated dynamically with 2800 rpm for 30 s and annealed at  $100^\circ\text{C}$  for 10 min, resulting in an active layer thickness  $\approx 180$  nm. PFN-Br was dissolved in methanol with a concentration of  $0.5 \text{ mg mL}^{-1}$ , filtered with a  $0.45 \mu\text{m}$  PDVF filter and spin-coated on top of the active layer dynamically with 2500 rpm for 30 s. Finally, 100 nm Ag were evaporated under high vacuum ( $\approx 5 \times 10^{-7}$  mbar). The device area was defined by a shadow mask and was  $0.16 \text{ cm}^2$ .

**Device Characterization:** JV measurements under 1 sun irradiation were performed with solar simulator from LOT Quantum Design and a Keithley 2450 was used as the source meter. As the samples were measured in a sealed box and the incident light was reflected two times at the glass window, current densities were corrected with additional 8%. Capacitance measurements were performed with a potentiostat Interface 1000 by the company Gamry Instruments to estimate thicknesses of the active layer in a non-destructive way. For this estimation the capacitance at high negative voltages ( $-3 \text{ V}$ ) was determined in the dark and a permittivity  $\epsilon_r$  of 3.9 was used. For low light measurements a warm white LED (CXA3050-0000-000N0YU227H) by the company Cree was used as a light source. According to manufacturer information the color temperature was  $2700 \text{ K}$ . To estimate the illumination for the JV measurements (which give the  $V_{\text{oc}}(J_{\text{sc}})$  and  $(FF)_{J_{\text{sc}}}$  pairs for the interpolation) a lux meter MS-200LED of the company Voltcraft was used. It was emphasized that the lux meter was only used for a rough estimation of the illuminance level and not to calculate efficiencies. The quantum efficiency measurements were performed with a home-made setup. A BENTHAM 605 lamp power supply powers the halogen and xenon lamp. A monochromator TM300 of the company BENTHAM had a symmetric Czerny–Turner geometry and used diffraction gratings. As well as for the JV measurements the current densities from  $Q_{\text{e}}$  measurements were also corrected with 8% refraction losses.

## Supporting Information

Supporting Information is available from the Wiley Online Library or from the author.

## Acknowledgements

The authors acknowledge funding from the state of Nordrhein-Westfalen via the project Enerscale and funding from the Helmholtz Association.

Open access funding enabled and organized by Projekt DEAL.

## Conflict of Interest

The authors declare no conflict of interest.

## Data Availability Statement

The data that support the findings of this study are available from the corresponding author upon reasonable request.

## Keywords

comparable efficiencies, indoor photovoltaics, non-fullerene acceptors, Shockley–Queisser limit indoors

Received: May 11, 2021

Revised: June 25, 2021

Published online: July 21, 2021

- [1] Y. Cui, H. Yao, J. Zhang, T. Zhang, Y. Wang, L. Hong, K. Xian, B. Xu, S. Zhang, J. Peng, Z. Wei, F. Gao, J. Hou, *Nat. Commun.* **2019**, *10*, 2515.
- [2] Y. Cui, H. Yao, J. Zhang, K. Xian, T. Zhang, L. Hong, Y. Wang, Y. Xu, K. Ma, C. An, C. He, Z. Wei, F. Gao, J. Hou, *Adv. Mater.* **2020**, *32*, 1908205.
- [3] Y. Lin, Y. Firdaus, F. H. Isikgor, M. I. Nugraha, E. Yengel, G. T. Harrison, R. Hallani, A. El-Labban, H. Faber, C. Ma, X. Zheng, A. Subbiah, C. T. Howells, O. M. Bakr, I. McCulloch, S. De Wolf, L. Tsetseris, T. D. Anthopoulos, *ACS Energy Lett.* **2020**, *5*, 2935.
- [4] Q. Liu, Y. Jiang, K. Jin, J. Qin, J. Xu, W. Li, J. Xiong, J. Liu, Z. Xiao, K. Sun, S. Yang, X. Zhang, L. Ding, *Sci. Bull.* **2020**, *65*, 272.
- [5] Y. Lin, M. I. Nugraha, Y. Firdaus, A. D. Scaccabarozzi, F. Aniés, A.-H. H. Emwas, E. Yengel, X. Zheng, J. Liu, W. Wahyudi, E. Yari, H. Faber, O. M. Bakr, L. Tsetseris, M. Heeney, T. D. Anthopoulos, *ACS Energy Lett.* **2020**, *5*, 3663.
- [6] Y. Cui, H. Yao, L. Hong, T. Zhang, Y. Tang, B. Lin, K. Xian, B. Gao, C. An, P. Bi, W. Ma, J. Hou, *Natl. Sci. Rev.* **2020**, *7*, 1239.
- [7] O. Almora, D. Baran, G. C. Bazan, C. Berger, C. I. Cabrera, K. R. Catchpole, S. Erten-Ela, F. Guo, J. Hauch, A. W. Y. Ho-Baillie, T. J. Jacobsson, R. A. J. Janssen, T. Kirchartz, N. Kopidakis, Y. Li, M. A. Loi, R. R. Lunt, X. Mathew, M. D. McGehee, J. Min, D. B. Mitzi, M. K. Nazeeruddin, J. Nelson, A. F. Nogueira, U. W. Paetold, N. Park, B. P. Rand, U. Rau, H. J. Snaith, E. Unger, et al., *Adv. Energy Mater.* **2021**, *11*, 2002774.
- [8] J. Gubbi, R. Buyya, S. Marusic, M. Palaniswami, *Future Gener. Comput. Syst.* **2013**, *29*, 1645.
- [9] L. Atzori, A. Iera, G. Morabito, *Comput. Networks* **2010**, *54*, 2787.
- [10] A. Al-Fuqaha, M. Guizani, M. Mohammadi, M. Aledhari, M. Ayyash, *IEEE Commun. Surv. Tutorials* **2015**, *17*, 2347.
- [11] H. Jayakumar, K. Lee, W. S. Lee, A. Raha, Y. Kim, V. Raghunathan, in *Proc. 2014 Int. Symp. Low Power Electronics and Design*, ACM, New York, NY **2014**, pp. 375–380.
- [12] I. Mathews, S. N. Kantareddy, T. Buonassisi, I. M. Peters, *Joule* **2019**, *3*, 1415.
- [13] H. Yu, Q. Yue, *Energy Procedia* **2012**, *16*, 1027.
- [14] H. K. H. Lee, Z. Li, J. R. Durrant, W. C. Tsoi, *Appl. Phys. Lett.* **2016**, *108*, 253301.
- [15] H. K. H. Lee, J. Wu, J. Barbé, S. M. Jain, S. Wood, E. M. Speller, Z. Li, F. A. Castro, J. R. Durrant, W. C. Tsoi, *J. Mater. Chem. A* **2018**, *6*, 5618.
- [16] M. Nam, H. Y. Noh, J. Cho, Y. Park, S. Shin, J. Kim, J. Kim, H. H. Lee, J. W. Shim, D. Ko, *Adv. Funct. Mater.* **2019**, *29*, 1900154.
- [17] S. Park, H. Ahn, J.-Y. Kim, J. B. Park, J. Kim, S. H. Im, H. J. Son, *ACS Energy Lett.* **2020**, *5*, 170.
- [18] Y. Xu, H. Yao, L. Ma, Z. Wu, Y. Cui, L. Hong, Y. Zu, J. Wang, H. Y. Woo, J. Hou, *Mater. Chem. Front.* **2021**, *5*, 893.
- [19] H. Yin, L. Ma, J. Yan, Z. Zhang, A. M. H. Cheung, J. Zhang, H. Yan, S. K. So, *Sol. RRL* **2020**, *4*, 2000291.
- [20] R. Arai, S. Furukawa, Y. Hidaka, H. Komiyama, T. Yasuda, *ACS Appl. Mater. Interfaces* **2019**, *11*, 9259.
- [21] C. H. Chen, H. C. Ting, Y. Z. Li, Y. C. Lo, P. H. Sher, J. K. Wang, T. L. Chiu, C. F. Lin, I. S. Hsu, J. H. Lee, S. W. Liu, K. T. Wong, *ACS Appl. Mater. Interfaces* **2019**, *11*, 8337.
- [22] C. Y. Liao, Y. Chen, C. C. Lee, G. Wang, N. W. Teng, C. H. Lee, W. L. Li, Y. K. Chen, C. H. Li, H. L. Ho, P. H. S. Tan, B. Wang, Y. C. Huang, R. M. Young, M. R. Wasielewski, T. J. Marks, Y. M. Chang, A. Facchetti, *Joule* **2020**, *4*, 189.
- [23] J. Liu, Y. Cui, Y. Zu, C. An, B. Xu, H. Yao, S. Zhang, J. Hou, *Org. Electron.* **2020**, *85*, 105798.
- [24] J. Luke, L. Corrêa, J. Rodrigues, J. Martins, M. Daboczi, D. Bagnis, J. Kim, *Adv. Energy Mater.* **2021**, *11*, 2003405.
- [25] S.-C. Shin, C. W. Koh, P. Vincent, J. S. Goo, J.-H. Bae, J.-J. Lee, C. Shin, H. Kim, H. Y. Woo, J. W. Shim, *Nano Energy* **2019**, *58*, 466.
- [26] H. Yin, J. K. W. Ho, S. H. Cheung, R. J. Yan, K. L. Chiu, X. Hao, S. K. So, *J. Mater. Chem. A* **2018**, *6*, 8579.
- [27] R. Singh, C. L. Chochos, V. G. Gregoriou, A. D. Nega, M. Kim, M. Kumar, S. C. Shin, S. H. Kim, J. W. Shim, J. J. Lee, *ACS Appl. Mater. Interfaces* **2019**, *11*, 36905.
- [28] R. Singh, T. Duan, Z. Kan, C. L. Chochos, G. P. Kini, M. Kumar, J. Park, J. Lee, J.-J. Lee, *Nano Energy* **2020**, *75*, 104934.
- [29] Y. You, C. E. Song, Q. V. Hoang, Y. Kang, J. S. Goo, D. Ko, J. Lee, W. S. Shin, J. W. Shim, *Adv. Funct. Mater.* **2019**, *29*, 1901171.
- [30] Y. Cui, H. Yao, T. Zhang, L. Hong, B. Gao, K. Xian, J. Qin, J. Hou, *Adv. Mater.* **2019**, *31*, 1904512.
- [31] Y. Cui, Y. Wang, J. Bergqvist, H. Yao, Y. Xu, B. Gao, C. Yang, S. Zhang, O. Inganäs, F. Gao, J. Hou, *Nat. Energy* **2019**, *4*, 768.
- [32] S. V. Dayneko, M. Pahlevani, G. C. Welch, *ACS Appl. Mater. Interfaces* **2019**, *11*, 46017.
- [33] Z. Ding, R. Zhao, Y. Yu, J. Liu, *J. Mater. Chem. A* **2019**, *7*, 26533.
- [34] H. Il Je, E. Y. Shin, K. J. Lee, H. Ahn, S. Park, S. H. Im, Y. H. Kim, H. J. Son, S. K. Kwon, *ACS Appl. Mater. Interfaces* **2020**, *12*, 23181.
- [35] L. K. Ma, Y. Chen, P. C. Y. Y. Chow, G. Zhang, J. Huang, C. Ma, J. Zhang, H. Yin, A. M. Hong Cheung, K. S. Wong, S. K. So, H. Yan, A. Man, H. Cheung, K. S. Wong, S. Kong, C. Ma, J. Zhang, H. Yin, A. M. Hong Cheung, K. S. Wong, S. K. So, H. Yan, *Joule* **2020**, *4*, 1486.
- [36] Y. Guo, W. Sato, K. Shoyama, H. Halim, Y. Itabashi, R. Shang, E. Nakamura, *J. Am. Chem. Soc.* **2017**, *139*, 9598.
- [37] M. Li, C. Zhao, Z. Wang, C. Zhang, H. K. H. Lee, A. Pockett, J. Barbé, W. C. Tsoi, Y. Yang, M. J. Carnie, X. Gao, W. Yang, J. R. Durrant, L. Liao, S. M. Jain, *Adv. Energy Mater.* **2018**, *8*, 1801509.
- [38] H. K. H. Lee, J. Barbé, S. M. P. Meroni, T. Du, C.-T. Lin, A. Pockett, J. Troughton, S. M. Jain, F. De Rossi, J. Baker, M. J. Carnie, M. A. McLachlan, T. M. Watson, J. R. Durrant, W. C. Tsoi, *Sol. RRL* **2019**, *3*, 1800207.
- [39] R. Cheng, C. Chung, H. Zhang, F. Liu, W. Wang, Z. Zhou, S. Wang, A. B. Djurišić, S. Feng, *Adv. Energy Mater.* **2019**, *9*, 1901980.
- [40] J. W. Lim, H. Kwon, S. H. Kim, Y.-J. You, J. S. Goo, D.-H. Ko, H. J. Lee, D. Kim, I. Chung, T. G. Kim, D. H. Kim, J. W. Shim, *Nano Energy* **2020**, *75*, 104984.
- [41] H. Sun, K. Deng, Y. Jiang, J. Ni, J. Xiong, L. Li, *Small* **2020**, *16*, 1906681.
- [42] M. Lee, E. Choi, A. M. Soufiani, J. Lim, M. Kim, D. Chen, M. A. Green, J. Seidel, S. Lim, J. Kim, X. Dai, R. Lee-Chin, B. Zheng, Z. Hameiri, J. Park, X. Hao, J. S. Yun, *Adv. Funct. Mater.* **2021**, *31*, 2008908.
- [43] X. He, J. Chen, X. Ren, L. Zhang, Y. Liu, J. Feng, J. Fang, K. Zhao, S. (Frank) Liu, *Adv. Mater.* **2021**, *33*, 2100770.
- [44] Y. C. Liu, H. H. Chou, F. Y. Ho, H. J. Wei, T. C. Wei, C. Y. Yeh, *J. Mater. Chem. A* **2016**, *4*, 11878.
- [45] M. Freitag, J. Teuscher, Y. Saygili, X. Zhang, F. Giordano, P. Liska, J. Hua, S. M. Zakeeruddin, J.-E. Moser, M. Grätzel, A. Hagfeldt, *Nat. Photonics* **2017**, *11*, 372.
- [46] Y. S. Tingare, N. S. Vinh, H.-H. Chou, Y.-C. Liu, Y.-S. Long, T.-C. Wu, T.-C. Wei, C.-Y. Yeh, *Adv. Energy Mater.* **2017**, *7*, 1700032.
- [47] K. S. K. Reddy, Y. C. Liu, H. H. Chou, K. Kala, T. C. Wei, C. Y. Yeh, *ACS Appl. Mater. Interfaces* **2018**, *10*, 39970.



- [48] M. L. Jiang, J. J. Wen, Z. M. Chen, W. H. Tsai, T. C. Lin, T. J. Chow, Y. J. Chang, *ChemSusChem* **2019**, 12, 3654.
- [49] R.-Y. Huang, W.-H. Tsai, J.-J. Wen, Y. J. Chang, T. J. Chow, *J. Power Sources* **2020**, 458, 228063.
- [50] E. Tanaka, H. Michaels, M. Freitag, N. Robertson, *J. Mater. Chem. A* **2020**, 8, 1279.
- [51] C. Y. Chen, Z. H. Jian, S. H. Huang, K. M. Lee, M. H. Kao, C. H. Shen, J. M. Shieh, C. L. Wang, C. W. Chang, B. Z. Lin, C. Y. Lin, T. K. Chang, Y. Chi, C. Y. Chi, W. T. Wang, Y. Tai, M. De Lu, Y. L. Tung, P. T. Chou, W. T. Wu, T. J. Chow, P. Chen, X. H. Luo, Y. L. Lee, C. C. Wu, C. M. Chen, C. Y. Yeh, M. S. Fan, J. De Peng, K. C. Ho, et al., *J. Phys. Chem. Lett.* **2017**, 8, 1824.
- [52] A. Virtuani, E. Lotter, M. Powalla, *Sol. Energy Mater. Sol. Cells* **2006**, 90, 2141.
- [53] F. Chen, *Adv. Opt. Mater.* **2019**, 7, 1800662.
- [54] H. S. Ryu, S. Y. Park, T. H. Lee, J. Y. Kim, H. Y. Woo, *Nanoscale* **2020**, 12, 5792.
- [55] R. Steim, T. Ameri, P. Schilinsky, C. Waldauf, G. Dennler, M. Scharber, C. J. Brabec, *Sol. Energy Mater. Sol. Cells* **2011**, 95, 3256.
- [56] C. M. Proctor, T.-Q. Nguyen, *Appl. Phys. Lett.* **2015**, 106, 083301.
- [57] S. Zeiske, O. J. Sandberg, N. Zarrabi, W. Li, P. Meredith, A. Armin, *Nat. Commun.* **2021**, 12, 3603.
- [58] B. P. Lechêne, M. Cowell, A. Pierre, J. W. Evans, P. K. Wright, A. C. Arias, *Nano Energy* **2016**, 26, 631.
- [59] Y. Cui, L. Hong, J. Hou, *ACS Appl. Mater. Interfaces* **2020**, 12, 38815.
- [60] C. L. Cutting, M. Bag, D. Venkataraman, *J. Mater. Chem. C* **2016**, 4, 10367.
- [61] B. Minnaert, P. Veelaert, *Energies* **2014**, 7, 1500.
- [62] Y. Cui, L. Hong, T. Zhang, H. Meng, H. Yan, F. Gao, J. Hou, *Joule* **2021**, 5, 1016.
- [63] H. Yin, S. Chen, S. H. Cheung, H. W. Li, Y. Xie, S. W. Tsang, X. Zhu, S. K. So, *J. Mater. Chem. C* **2018**, 6, 9111.
- [64] Y. Cho, T. Kumari, S. Jeong, S. M. Lee, M. Jeong, B. Lee, J. Oh, Y. Zhang, B. Huang, L. Chen, C. Yang, *Nano Energy* **2020**, 75, 104896.
- [65] C. I. d. l'Eclairage (CIE), CIE standard illuminant (CIE S 017:2020 ILV/17-23-021)," <http://cie.co.at/eilvterm/17-23-021> (accessed: July 2021).
- [66] I. Fryc, P. Tabaka, *Opt. Appl.* **2019**, 49, 345.
- [67] H. Zheng, D. Li, C. Ran, Q. Zhong, L. Song, Y. Chen, P. Müller-Buschbaum, W. Huang, *Sol. RRL* **2021**, 5, 2100042.
- [68] M. Saliba, L. Etgar, *ACS Energy Lett.* **2020**, 5, 2886.
- [69] P. M. Sommeling, H. C. Rieffe, J. A. M. van Roosmalen, A. Schönecker, J. M. Kroon, J. A. Wienke, A. Hinsch, *Sol. Energy Mater. Sol. Cells* **2000**, 62, 399.
- [70] D. J. Wehenkel, K. H. Hendriks, M. M. Wienk, R. A. J. Janssen, *Org. Electron.* **2012**, 13, 3284.
- [71] P. Hartnagel, T. Kirchartz, *Adv. Theory Simul.* **2020**, 3, 2000116.
- [72] S. Beuel, P. Hartnagel, T. Kirchartz, *Adv. Theory Simul.* **2021**, 4, 2000319.
- [73] L. Hong, H. Yao, Z. Wu, Y. Cui, T. Zhang, Y. Xu, R. Yu, Q. Liao, B. Gao, K. Xian, H. Y. Woo, Z. Ge, J. Hou, *Adv. Mater.* **2019**, 31, 1903441.
- [74] W. Shockley, H. J. Queisser, *J. Appl. Phys.* **1961**, 32, 510.
- [75] P. W. Bridgman, *Phys. Rev.* **1928**, 31, 101.
- [76] M. F. Müller, M. Freunek, L. M. Reindl, *IEEE J. Photovoltaics* **2013**, 3, 59.
- [77] J. K. W. Ho, H. Yin, S. K. So, *J. Mater. Chem. A* **2020**, 8, 1717.
- [78] N. H. Reich, W. G. J. H. M. van Sark, E. A. Alsema, R. W. Lof, R. E. I. Schropp, W. C. Sinke, W. C. Turkenburg, *Sol. Energy Mater. Sol. Cells* **2009**, 93, 1471.
- [79] N. H. Reich, W. Van Sark, E. a Alsema, S. Y. Kan, S. Silvester, A. Van Der Heide, R. W. Lof, R. Schropp, in *Proc 20th European Photovoltaic Solar Energy Conf.*, EU PVSEC, München, Germany **2005**.
- [80] S. W. Glunz, J. Dicker, M. Esterle, M. Hermle, J. Isenberg, F. J. Kamerwerd, J. Knobloch, D. Kray, A. Leimenstoll, F. Lutz, D. Oßwald, R. Preu, S. Rein, E. Schäffer, C. Schetter, H. Schmidhuber, H. Schmidt, M. Steuder, C. Vorgrimler, G. Willeke, in *Conf. Record IEEE Photovoltaic Specialists Conf.*, IEEE, Piscataway, NJ **2002**.
- [81] T. Kirchartz, P. Kaienburg, D. Baran, *J. Phys. Chem. C* **2018**, 122, 5829.
- [82] J. Yao, T. Kirchartz, M. S. Vezie, M. A. Faist, W. Gong, Z. He, H. Wu, J. Troughton, T. Watson, D. Bryant, J. Nelson, *Phys. Rev. Appl.* **2015**, 4, 014020.
- [83] T. Kirchartz, K. Taretto, U. Rau, *J. Phys. Chem. C* **2009**, 113, 17958.
- [84] J. Wong, S. T. Omelchenko, H. A. Atwater, *ACS Energy Lett.* **2021**, 6, 52.
- [85] L. J. A. Koster, S. E. Shaheen, J. C. Hummelen, *Adv. Energy Mater.* **2012**, 2, 1246.
- [86] M. Azzouzi, T. Kirchartz, J. Nelson, *Trends Chem.* **2019**, 1, 49.
- [87] S. Liu, J. Yuan, W. Deng, M. Luo, Y. Xie, Q. Liang, Y. Zou, Z. He, H. Wu, Y. Cao, *Nat. Photonics* **2020**, 14, 300.
- [88] X.-K. Chen, D. Qian, Y. Wang, T. Kirchartz, W. Tress, H. Yao, J. Yuan, M. Hülsbeck, M. Zhang, Y. Zou, Y. Sun, Y. Li, J. Hou, O. Inganäs, V. Coropceanu, J.-L. Bredas, F. Gao, *Nat. Energy* **2021**, <https://doi.org/10.1038/s41560-021-00843-4>.
- [89] F. D. Eisner, M. Azzouzi, Z. Fei, X. Hou, T. D. Anthopoulos, T. J. S. Dennis, M. Heeney, J. Nelson, *J. Am. Chem. Soc.* **2019**, 141, 6362.
- [90] U. Rau, B. Blank, T. C. M. Müller, T. Kirchartz, *Phys. Rev. Appl.* **2017**, 7, 044016.
- [91] X. Hou, Y. Wang, H. K. H. Lee, R. Datt, N. Uslar Miano, D. Yan, M. Li, F. Zhu, B. Hou, W. C. Tsoi, Z. Li, *J. Mater. Chem. A* **2020**, 8, 21503.
- [92] N. An, Y. Cai, H. Wu, A. Tang, K. Zhang, X. Hao, Z. Ma, Q. Guo, H. S. Ryu, H. Y. Woo, Y. Sun, E. Zhou, *Adv. Mater.* **2020**, 32, 2002122.
- [93] W. Gao, H. Fu, Y. Li, F. Lin, R. Sun, Z. Wu, X. Wu, C. Zhong, J. Min, J. Luo, H. Y. Woo, Z. Zhu, A. K. Y. Jen, *Adv. Energy Mater.* **2021**, 11, 2003177.